A FREE WAKE METHOD FOR VERTICAL-AXIS WIND TURBINE PERFORMANCE PREDICTION

H. DUMITRESCU[*,**], V. CARDOŞ[*]

Based on the lifting line theory and a free vortex wake model, a method including dynamic stall effects is presented for predicting the performance of a three-dimensional vertical-axis wind turbine. A vortex model is used in which the wake is composed of trailing streamwise and shedding spanwise vortices, whose strengths are equal to the change in the bound vortex strength as dictated by Helmholtz and Kelvin's theorems. Performance parameters are calculated by application of the Biot-Savart law along with the Kutta-Joukowski theorem and a semi-empirical dynamic stall model. Predictions are shown to compare favorably with existing experimental data. The method can predict local and global performances more accurately than the previous models.

1. INTRODUCTION

Because of the complex nature of the unsteady flowfield in which vertical-axis wind turbines must operate, determination of the aerodynamic performance can be quite difficult. Development of a method for predicting machine performance over the complete range of wind speeds without recourse to certain simplifying assumptions is doubtful. Clearly, accuracy of the performance estimates depends largely on the validity of the assumptions employed and on the rigor of the method of analysis adopted.

Methods concerned with the prediction of aerodynamic loading and performance of vertical-axis wind turbine, have been formulated by a number of authors. Classification of the methods is based on the manner in which the induced velocity at a blade section is evaluated.

Simple aerodynamic stream tube models are based on the conservation of momentum principle in a quasisteady flow, by equating the forces on the rotor blades to the change in streamwise momentum through the rotor. They include three categories of analytical model: the single-streamtube model [1], which assumes that the entire rotor is enclosed in one streamtube model which assumes that the entire rotor is enclosed in one streamtube; the multiple-streamtube model [2], in which the swept volume of rotor is divided into a series of adjacent streamtubes and the double-multiple streamtube model [3], which replace the rotor by two actuator disks in tandem aerodynamically independent. The overall

performance can be predicted reasonably well with these models under conditions where the rotor blades are lightly loaded and the rotor tip to wind speed rations are not high. However, the predicted blade loads are inaccurate since these models assume: a quasi-steady flow through the rotor, a constant or unreal streamwise velocity as a function of streamwise position in the vicinity of the rotor, and zero normal velocities to the freestream direction. In addition, for large tip to wind speed ratios accurate performance predictions cannot be made because the momentum equations used in these models become invalid.

Vortex models are more involved as the induced velocity is determined from an analysis of the flowfield created by the vortex system in the rotor wake. Vortex methods can account for a finite number of blades, can account for blade span effects (lifting line theories) or for blade chord effects (lifting surface theories) and can alleviate all of the noted objections for the momentum models. Several vortex models for vertical-axis wind turbines [4–7] have been developed in the past, although none are applicable to predict dynamic stall that is of crucial importance for optimizing the Darrieus turbines.

In the case of the Darrieus wind turbine, when the operational wind speed approaches its maximum, all blade sections exceed the static-stall incidence, the angle of attack (α) changes rapidly, and the whole blade works in dynamic-stall conditions. When the angle of attack gets too large, the wind flow separates from the leading edge, causing the airfoil to stall or lose lift. Dynamic stall overdrives aerodynamic lift force when α is rapidly increasing, and underdrives lift when α is rapidly decreasing. The sharp changes in aerodynamic forces significantly increase unsteady blade loads that can be very damaging to the wind turbine structure. Another contribution to the unsteady aerodynamics of the Darrieus rotor is dynamic stall, which occurs at low tip-speed ratios (*e.g.*, during starting and stopping) or in sudden gusts, and its effects are very significant in drive-train calculations, generator sizing, and overall system design. Therefore, the attempt to predict dynamic stall is uncommon one.

The unsteady aerodynamic response of the blade aerodynamics to the cyclic variation of incidence in Darrieus motion can be achieved by superposition of a basic vortex method with the semi-empirical dynamic stall model of Leishman and Beddoes [8]. The present work combines these two high-quality techniques to produce a comprehensive aerodynamic model. Although both techniques have been applied separately in the past, the new hybrid method for vertical-axis wind turbine performance prediction is a unique combination of the two.

2. AERODYNAMIC ANALYSIS

Vortex Model. The local air velocity relative to a rotor blade consists of the free-stream velocity that due to the blade motion and the wake induced velocity. In order to predict the inflow at the blades, it is necessary to describe the blade surfaces and the wake. The blades are simply lifting surfaces of finite span, so that

each blade of the rotor is represented by a bound vortex lifting line, located along the rotor blade quarter chord line, with a spanwise varying concentrated circulation strength. The wake consists of trailing streamwise and shedding spanwise vortex filaments resulted from the spanwise and temporal variation in loading distributions on the blades, as required by the circulation conservation theorems (Helmholtz and Kelvin's theorems). This vortex system associated with a blade element is shown in Fig. 1.
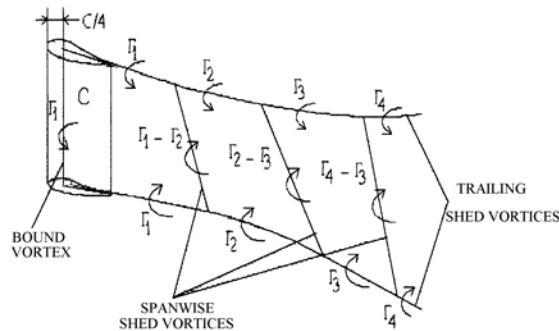

Fig. 1 – Vortex model of the blade element.

The complexity of flowfield precludes any hope of a closed form solution; hence a numerical method employing vortex panel technique is used. The numerical model of the blades consists of spanwise distributed panels, each of which is considered as having a constant vortex strength, concentrated into a straight-line vortex segment at a quarter chord behind the leading edge. Each resulting panel contains a control point located on the local chord at the middle of panel and at three-quarters of the chord behind the leading edge. One requirement of this piece-wise constant representation is that the spanwise segments be small enough so that straight-line segments adequately represent the curvature variation of blade.

The wake consists of a system of shedding and trailing vortices, the strength of which reflects any change in bound vortex with respect to time and position along the blade. In order to model the wake an unsteady vortex lattice method, based on the marching-vortex concept, is used. So, the motion begins from an impulsive start from rest with the subsequent generation of spanwise and trailing vortices from each bond vortex according to Kelvin's theorem, modeled by a sequence of quadrilateral vortex systems with constant strength along each side, shed at equal time intervals. The wake contains a finite number of points whose motion describes vortex end-point deformation. These points are taken to be connected by straight-line vortex segments, which represented the distortion. Therefore, no deformation of the vortex segments from a straight line is permitted, and the spanwise and trailing vortices are laid down in a finite number of straight-

line segments forming the wake lattice which describe the wake motion. Each wake lattice point is identified by a double subscript (i, j) which denote the origin blade node and the origin time step of the wake lattice points. Thus, at each time step j, the new strengths of each vortex quadrilateral, just aft of the trailing edge (Fig. 2), can be written as
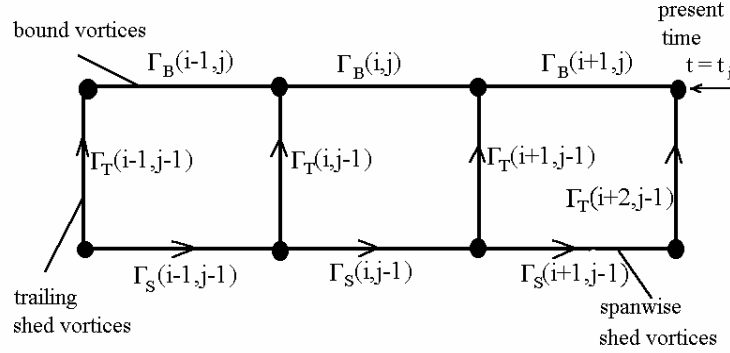

Fig. 2 – Vortex ring shedding model.

$$\Gamma_S\left(i, j-1\right) = \Gamma_B\left(i, j-1\right) - \Gamma_B\left(i, j\right)$$
$$\Gamma_T\left(i, j-1\right) = \Gamma_B\left(i, j\right) - \Gamma_B\left(i-1, j\right). \tag{1}$$

The wake points are assumed to move downstream with the local fluid velocities given by

$$\vec{V}\left(i, j\right) = \vec{V}_\infty + \vec{v}_I\left(i, j\right), \tag{2}$$

where $\vec{V}_\infty$ is the undisturbed freestream velocity and $\vec{v}_I\left(i, j\right)$ is induced velocity by all of straight-line vortex segments in the flow field.

The induced velocity at the wake lattice points is computed by application of the Biot-Savart law.

Governing Equations. According to the Biot-Savart law, the velocity induced by a vortex filaments of strength Γ and length l, at a point C not on the filament, is given by

$$\vec{v}_I\left(C\right) = \frac{\Gamma}{4\pi} \int_l \frac{\vec{r} \times \mathrm{d}\vec{l}}{r^3}, \tag{3}$$

where $\mathrm{d}\vec{l}$ is an element of the vortex filament and $\vec{r}$ is the position vector from point C to the element $\mathrm{d}\vec{l}$. For a straight line vortex segment with end points at A and B equation (3) yields

$$\vec{v}_I(C) = \frac{\Gamma}{4\pi} \frac{\vec{r}_{CA} \times \vec{l}}{\left|\vec{r}_{CA} \times \vec{l}\right|^2} = \left(\frac{\vec{l} \cdot \vec{r}_{CB}}{\left|\vec{r}_{CB}\right|} - \frac{\vec{l} \cdot \vec{r}_{CA}}{\left|\vec{r}_{CA}\right|} \right), \tag{4}$$

where the local vectors $\vec{r}_{CA}, \vec{r}_{CB}$ (the position vectors of points A, B relative to the point C) and $\vec{l}$ can be expressed in terms of the position vectors of points A, B and C from the origin.

$$\begin{Bmatrix} \vec{l} \\ \vec{r}_{CB} \\ \vec{r}_{CA} \end{Bmatrix} = \begin{bmatrix} -1 & 1 & 0 \\ 0 & 1 & -1 \\ 1 & 0 & -1 \end{bmatrix} \cdot \begin{Bmatrix} \vec{r}_{OA} \\ \vec{r}_{OB} \\ \vec{r}_{OC} \end{Bmatrix}. \tag{5}$$

The points A, B and C can be defined in terms of lattice point notation such as: $C \equiv (i, j)$ is the lattice point at which the velocity is computed, $A \equiv (k, l+1)$ and $B \equiv (k+1, l)$ are the end points of any spanwise vortex segment, $A \equiv (k, l)$ and $B \equiv (k, l+1)$ are the end points of any trailing vortex segment.

The total disturbance velocity at any lattice point (i, j) is then obtained by summing the induced velocities resulting from all vortex segments representing the blades and wake

$$\vec{v}_I(i, j) = \sum_{k=1}^{NB} \sum_{l=1}^{NT-1} \vec{V}_{ITV} + \sum_{k=1}^{NB-1} \sum_{l=1}^{NT} \vec{V}_{ISV}, \tag{6}$$

where: V_{ITV} is the velocity induced by the trailing vortices; V_{ITS} is the velocity induced by spanwise (bound and shed) vortices; NB is the number of blade element end-points; NT is the number of time steps.

The closure of the vortex model is the relationship for the bound vortex strength (Γ_B) which can be related to the local relative air velocity (V_{rel}), section chord (c) and section lift coefficient ($C_L(\alpha)$) through the Kutta-Joukowski law

$$\Gamma_B = \frac{1}{2} C_L c V_{rel}. \tag{7}$$

The local relative velocity in the plane of the airfoil section (V_{rel}) and local airfoil angle of attack (α) are function of the local tangential velocity of the blade element (U_T), the induced velocity at the control point on the blade element ($\vec{v}_I(u, v, w)$), the wind velocity (V_∞) and the blade azimuthal angle (θ). Referring to Fig. 3, the following relationships can be obtained

$$\vec{V}_{rel} = \left(V_\infty + u + U_T \cos\theta\right)\vec{i} + v\vec{j} + \left(w - U_T \sin\theta\right)\vec{k}, \tag{8}$$

$$V_{rel} = \left[\left(\vec{V}_{rel}\vec{n}\right)^2 + \left(\vec{V}_{rel}\vec{t}\right)^2 \right]^{1/2}, \tag{9}$$

$$\alpha = \tan^{-1} \frac{\vec{V}_{rel}\vec{n}}{\vec{V}_{rel}\vec{t}}, \tag{10}$$

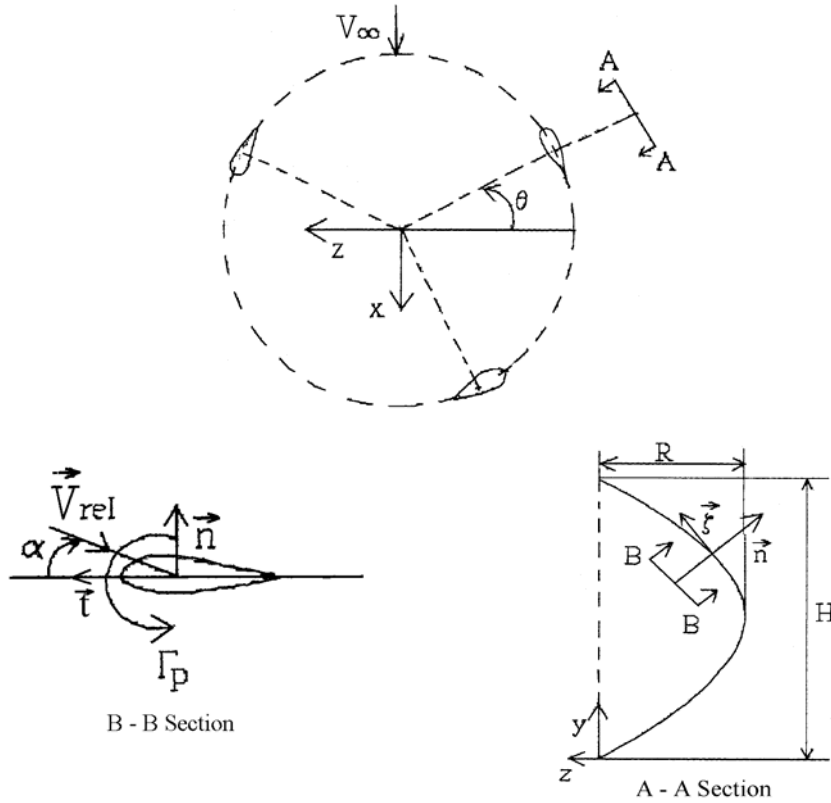$$U_T = r\Omega. \tag{11}$$

Fig. 3 – Rotor and blade coordinate system.

Unlike the vortex methods developed in the past based on steady airfoil data for the lift and drag coefficients, the present method utilizes semi-empirical dynamic stall model of Leishmann and Beddoes [8] to predict unsteady aerodynamic characteristics for the blade sections. Thus the effects of dynamic stall are automatically introduced into eq. (7) through the section lift coefficient. The blade airfoil section tangential and normal-force coefficients C_T and C_N can be written

$$C_T = C_L \sin\alpha - C_D \cos\alpha, \tag{12}$$

$$C_N = -C_L \cos\alpha - C_D \sin\alpha,$$

where the section lift and drag coefficients C_L and C_D are also yielded by the dynamic stall model.

The instantaneous values of the blade tangential and normal-forces, rotor torque and power can be then written in nondimensional form as

$$F_T^+ = \frac{F_T}{1/2\rho S V_\infty^2} = \frac{cH}{S} \sum_{i=1}^{NB-1} \left(\frac{l}{H}\right)_i C_{Ti} \left(\frac{V_{rel}}{V_\infty}\right)_i^2,$$

(13)

$$F_N^+ = \frac{F_N}{1/2\rho S V_\infty^2} = \frac{cH}{S} \sum_{i=1}^{NB-1} \left(\frac{l}{H}\right)_i C_{Ni} \left(\frac{V_{rel}}{V_\infty}\right)_i^2,$$

(14)

$$C_Q^+ = \frac{Q}{1/2\rho R S V_\infty^2} = \frac{cH}{S} \sum_{i=1}^{NB-1} \left(\frac{l}{H}\right)_i C_{Ti} \left(\frac{r}{R}\right)_i \left(\frac{V_{rel}}{V_\infty}\right)_i^2,$$

(15)

$$C_P^+ = \frac{P}{1/2\rho S V_\infty^3} = \frac{cH\lambda_{eq}}{S} \sum_{i=1}^{NB-1} \left(\frac{l}{H}\right)_i C_{Ti} \left(\frac{r}{R}\right)_i \left(\frac{U_{rel}}{V_\infty}\right)_i^2,$$

(16)

where S is the rotor-swept area, H is the height of the rotor and λ_{eq} is the tip-speed ratio at the equator. The average power coefficient for the entire rotor during a single revolution is given by

$$C_P = \frac{1}{\text{NTI}} \sum_{j=1}^{\text{NTI}} C_{Pj}^+ ,$$

(17)

where NTI is the number of time steps per revolution of the rotor.

Numerical Procedure. For the present free wake-lifting line blade method, the unknowns of the problem are both spanwise bound circulation distribution and wake geometry. The above aerodynamic relationships result in a system of simultaneous non-linear equations in terms of the unknown blade circulation distribution and wake geometry. Since the wake geometry is not a priori known, the numerical procedure requires that calculations be made at successive small time steps until a periodic solution is built up. Initially there is no wake structure and it is only as the wake develops sufficiently that a periodic solution is obtained. Therefore, the wake geometry is computed employing a time-stepping procedure, and the solution for the circulation strength is then obtained at each time step using an iterative matrix solution method.

The numerical procedure begins with no wake structure and zero bound vorticity distribution (*i.e.* zero induced velocities). The bound vortex strength and the last value of the induced velocity are then calculated for each segment using eqs. (7–11) and eq. (6) respectively. The process is repeated until consistent values are obtained for the induced velocities and bound vortices. The computation for this time step is ended by the calculation of the instantaneous blade forces and rotor performance (torque and power output) from eqs. (13–14) and eqs. (15–16)

respectively, the calculation of the induced velocities at each wake lattice point using eq. (6) and the calculation of the new positions of all of the wake vortex segments using eq. (5). Time is increased and a new set of shed vortices is created using eq. (1). The foregoing procedure may be repeated to obtain the solution at future times. If a revolution has been completed the rotor performance for the revolution is output. The vortex wake is truncated after a periodic solution is achieved (*i.e.*, ten rotor revolutions). In order to reduce the computational effort the wake is frozen after two revolutions of the rotor (it is simply convicted there after with the freestream velocity).

3. RESULTS AND DISCUSSIONS

This section presents a selection of results obtained by both the three-dimensional vortex model (3-DVM) described previously and an improved code based on double-multiple streamtube model (DMSTM) [9]. The corresponding results are compared with the experimental data on the Sandia 17-m wind turbine configuration [10]. The dynamic stall is simulated by the indicial model for both aerodynamic codes.

Local Aerodynamic Coefficients. The distribution of local normal force coefficient C_N at the equator level is plotted as a function of the azimuth angle θ for values of tip-speed ratio λ_{eq} varying from 2.33 to 4.60 for the Sandia 17-m wind turbine rotating at 38.7 rpm according to the experimental data (Figs. 4–6). Figure 4 shows that vortex model represents quite accurately the distribution of the normal force coefficient for almost all azimuth angle values. However, near $\theta \approx -120$ deg. in the downwind zone, predictions are different from experimental data. Akins [10], in his experimental data analysis, has compared the experimental data to values predicted by a vortex model coupled with Gormont dynamic stall model. He concluded that the wake interaction in the downwind zone doesn't allow the establishment of dynamic stall. The present vortex model can not also predict this effect. With increasing tip-speed ratio ($\lambda_{eq} = 3.09$ and 4.60), this behaviour (due to wake interaction) tends to disappear and the values predicted by both models agree quite well with the corresponding experimental data. To better visualize the dynamic stall phenomena characterized by an hysteresis loop on normal force coefficient C_N curves vs. angle of attack α, in Fig. 7 it is presented the variation of this coefficient as function of the angle of attack for a tip-speed ratio $\lambda_{eq} = 2.49$ predicted by both models. Although both models point out the existence of the dynamic stall in the upwind part (hysteresis loop) and the similarity of boundary layer reattachment, the normal force coefficient predictions by the vortex model agree better to experimental data.
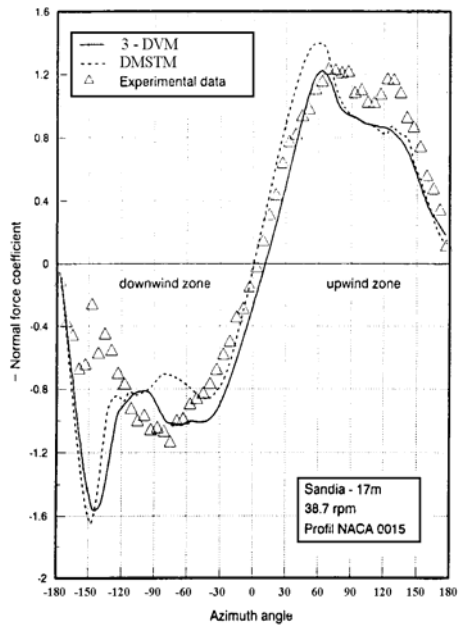
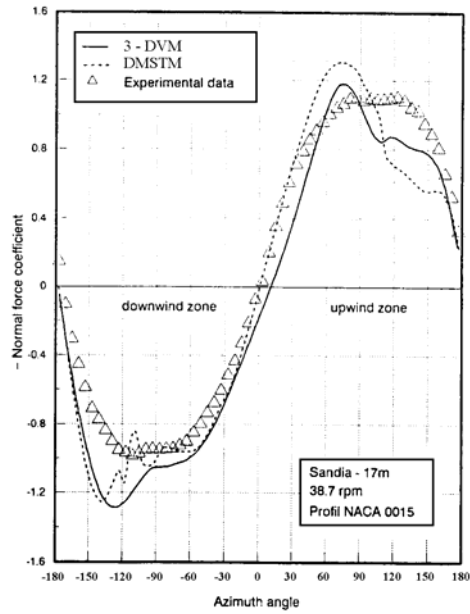Fig. 4 – Normal force coefficient *vs.* azimuth angle at 38.7 rpm and $\lambda_{eq.}$= 2.33.

Fig. 5 – Normal force coefficient *vs.* azimuth angle at 38.7 rpm and $\lambda_{eq.}$= 3.09.
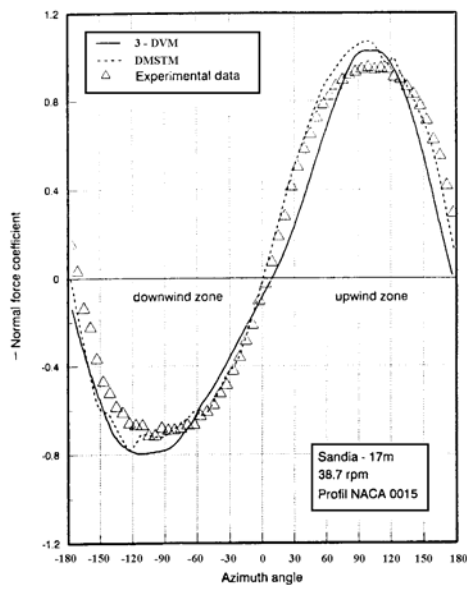

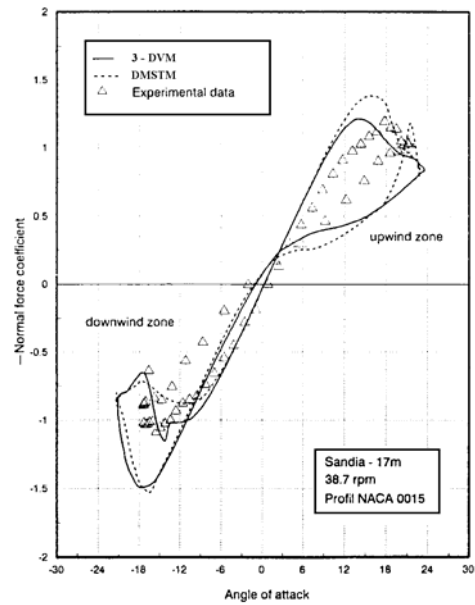Fig. 6 – Normal force coefficient *vs.* azimuth angle at 38.7 rpm and $\lambda_{eq.}$= 4.60.

Fig. 7 – Normal force coefficient *vs.* angle of attack at 38.7 rpm and $\lambda_{eq.}$= 2.49.

In Figs. 8–10 a comparison is shown between the local tangential force coefficients C_T as predicted by the two models and as obtained from experimental measurements. In general, it can be seen that the vortex model reproduces quite well the experimental data for all tips to wind speed ratios presented. It seems that the onset of dynamic stall gives a kind of irregularity to the curves of the tangential force coefficient, which tends to disappear with increasing tip-speed ratio (Figs. 9 and 10). The predictions of C_T by the streamtube model are in reasonable agreement with experimental data in the downwind zone, but in the upwind zone for $\theta > 150$ deg., they are completely different from the corresponding experimental data. Moreover, for almost all cases presented, this model overestimates the maximum value of the tangential force coefficient both in the upwind and downwind zone of the rotor.

Global Performance. A comparison between rotor power coefficients predicted by the two models and the experimental data for the Sandia 17-m wind turbine operating at 42.2 and 50.6 rpm is shown in Figs. 11 and 12. Even if the effect of dynamic stall is not really visible on power coefficient curves, however this kind of curves allows one to have a better idea about the accuracy of the results at low wind velocities while the power curves deals with greater wind velocities. In the dynamic stall zone ($1 < \lambda_{eq} < 4$) both models seem to reproduce quite accurately this zone, but in the transition zone ($4 < \lambda_{eq} < 6$) both models slightly underestimate the maximum value of the power coefficient. For the unstalled regime, it is obvious that the vortex model yields better predictions than the streamtube model.

Figure 12 illustrates a interesting comparison between several aerodynamic models: double-multiple streamtube model (DMSTM) [9], Strickland's vortex model (VDART 3) [6] and local circulation model (MCL) [11]. According with experimental data, the present vortex model provides a good representation of the power coefficient over the complete range of tip-speed ratios. However, it should be noted that the vortex models does not yield power coefficient predictions which are substantially better, than the streamtube models when they are compared to experimental data.

The dynamic stall phenomenon is clearly visible on the power curves characterized by a plateau at high speed. Comparison of rotor power values predicted by both models and experimental data is shown in Figs. 13 and 14. For low wind velocities ($V_{eq} < 10$ m/s), both models seem to give a good approximation of the experimental measurements of rotor power though in the dynamic stall regime ($V_{eq} > 12.5$ m/s) the DMSTM code using the indicial model does not predict an almost constant value and keeps on increasing. The vortex model predicts a plateau close to the experimental one for both rotational speeds of 42.2 rpm and 50.6 rpm.
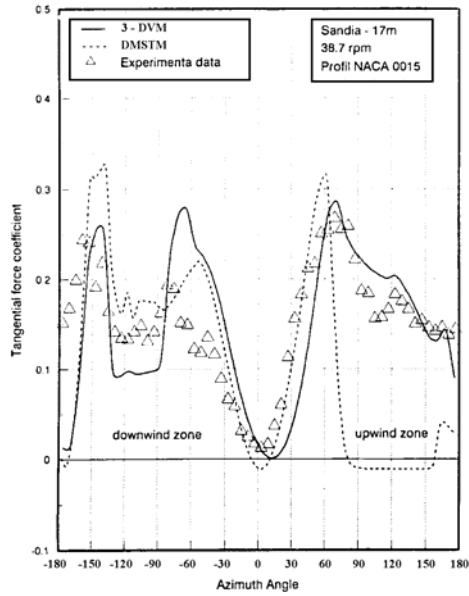
Fig. 8 – Tangential force coefficient *vs.* azimuth angle at 38.7 rpm and $\lambda_{eq.}= 2.33$.
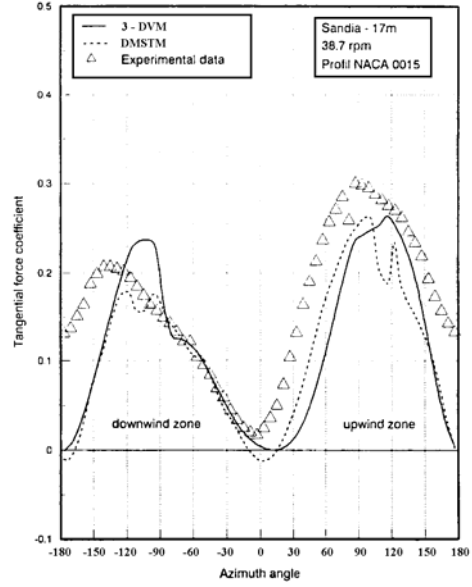

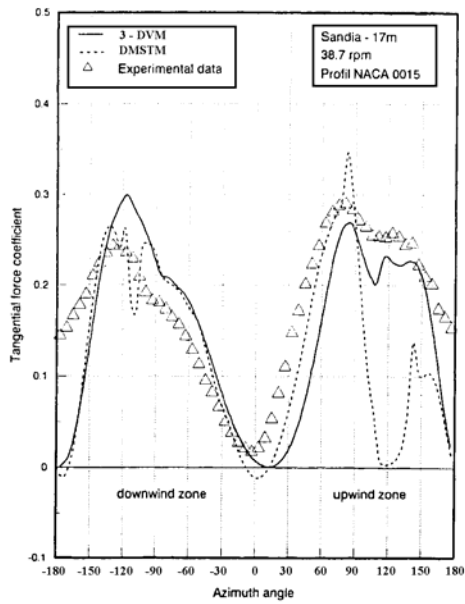Fig. 10 – Tangential force coefficient *vs.* azimuth angle at 38.7 rpm and $\lambda_{eq.}= 3.70$.

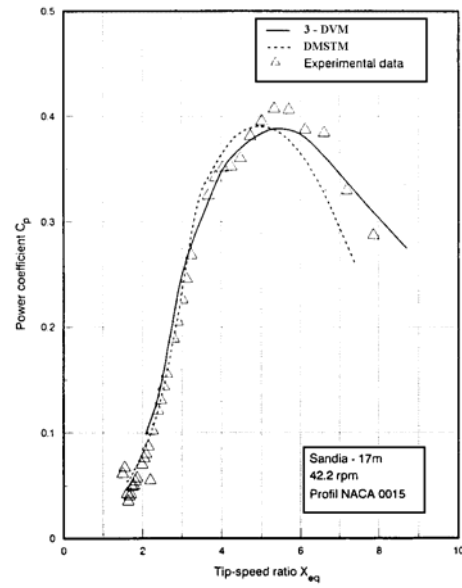Fig. 9 – Tangential force coefficient *vs.* azimuth angle at 38.7 rpm and $\lambda_{eq.}= 3.09$.

Fig. 11 – Power coefficient *vs.* tip-speed ratio for Sandia-17m at 42.2 rpm.
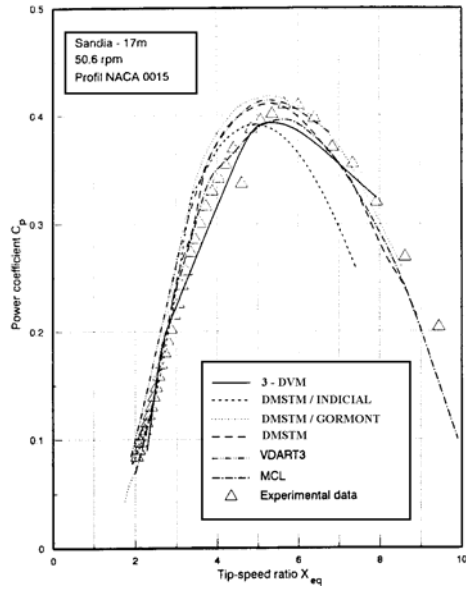
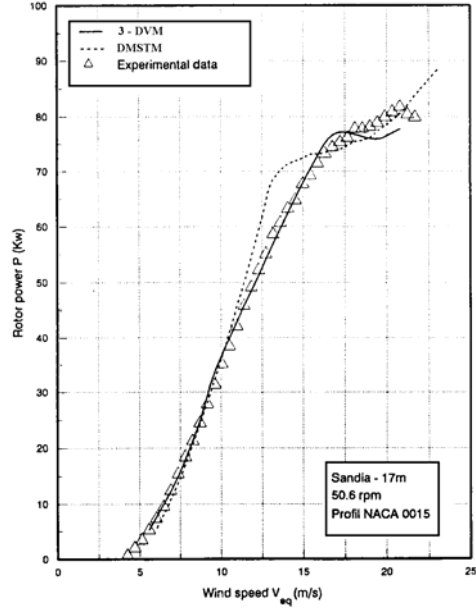Fig. 12 – Power coefficient *vs.* tip-speed ratio
for Sandia-17 m at 50.6 rpm.

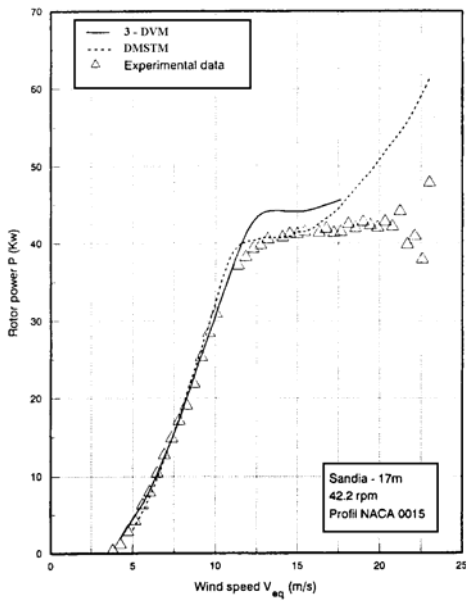Fig. 14 – Rotor power *vs.* wind speed
for Sandia-17 m at 50.6 rpm.

Fig. 13 – Rotor power *vs.* wind speed
for Sandia-17 m at 42.2 rpm.

4. CONCLUSIONS

The main objective of this study was to develop a new free wake method to analyze the global performance and unsteady blade loads of vertical-axis wind turbines. This has been accomplished by means of a three-dimensional unsteady aerodynamic solution based on a basic vortex flow coupled to an unsteady airfoil performance model. The numerical procedure implies a time marching scheme; according to that at each time step the strength of the bound circulation and latest wake are computed by using Kutta-Joukowski law and the previously shed wake vortices with unchanged strengths. Dynamic stall effects were simulated by an indicial model (as dynamic stall model) which tackles this problem at a more physical level of approximation but still in a sufficiently sample manner.

Analysis of the computed results presented in the previous section has demonstrated certain success of the vortex model coupled with the indicial model regarding its ability to accurately predict the instantaneous aerodynamic characteristics of Darrieus wind turbine. The results also tend to support the fact that among other semi-empirical models, the indicial model allows the best representation of dynamic stall for the prediction of wind turbine performance.

The vortex model yields results with regard to rotor wake velocities, which are at least in good qualitative agreement with flow visualization experiments. A more detailed experimental study of the turbine wake it is necessary too more rigorously validate the aerodynamic model.

Received November 1, 2000

REFERENCES

1. R. J. TEMPLIN, *Aerodynamic Performance Theory for the NRC Vertical-Axis Wind Turbine*, National Research Council of Canada, Rept. LTR-LA-160, June 1974.
2. J. H. STRICKLAND, *The Darrieus Turbine: A Performance Prediction Model Using Multiple Streamtube*, Sandia National Lab. Rept. SAND 75-0431, Oct. 1975.
3. I. PARASCHIVOIU, *Aerodynamic Loads and Performance of the Darrieus Rotor*, Journal of Energy, **6**, *6*, Nov.-Dec., 1982.
4. J. B. FANUCCI, R. E. WALTERS, *Innovative Wind Machines: The Theoretical Performances of a Vertical-Axis Wind Turbine*, Proceedings of the Vertical-Axis Wind Turbine Technology Workshop, Sandia Laboratory Report SAND 76-5586, May 1976.
5. O. HOLMES, *A Contribution to the Aerodynamic Theory of the Vertical-Axis Wind Turbine*, Proceedings of the International Symposium on Wind Energy Systems, St. John's College, Cambridge, England, September 1976.

6. J. H. STRICKLAND, B. T. WEBSTER, T. NGUYEN, *A Vortex Model of the Darrieus Turbine: An Analytical and Experimental Study*, Journal of Fluids Engineering, **101**, *4*, December 1979.

7. R. E. WILSON, S. N. WALKER, *Fixed Wake Analysis of the Darrieus Rotor*, Oregon State University, Mechanical Engineering Department, Contract 42-2967, 1980.

8. J. G. LEISHMAN, T. S. BEDDOES, *A Generalized Model for Airfoil Unsteady Aerodynamic Behaviour and Dynamic Stall using the Indicial Method*, Proceedings of the 42nd Annual Forum of the American Helicopter Society, Washington DC, 1986.

9. I. PARASCHIVOIU, *Double-Multiple Streamtube Model for Studying Vertical-Axis Wind Turbines*, Journal of Propulsion and Power, **4**, *4*, July-August 1988.

10. R. E. AKINS, *Measurements of Surface Pressure on an Operating Vertical-Axis Wind Turbine*, Contractor Report SAND 89-7051, Sandia National Laboratories, Albuquerque, New Mexico 87185, 1989.

11. B. MASSÉ, *A Local Circulation Model for Darrieus Vertical-Axis Wind Turbine*, Journal of Propulsion and Power, **2**, *2*, 1986.